Systematic effects induced by a flat isotropic dielectric slab

Claudio Macculi[*,1], Mario Zannoni[♯], Oscar Antonio Peverini[‡], Ettore Carretti[*,2], Riccardo Tascone[‡], Stefano Cortiglioni[*]

[*] *INAF-IASF Bologna, Via Gobetti 101, 40129 Bologna, Italy*
[♯] *Dip. di Fisica, Univ. di Milano - Bicocca, P.zza della Scienza 3, 20126 Milano, Italy*
[‡] *CNR-IEIIT, C.so Duca degli Abruzzi 24, 10129 Torino, Italy*

The instrumental polarization induced by a flat isotropic dielectric slab in microwave frequencies is faced. We find that, in spite of its isotropic nature, such a dielectric can produce spurious polarization either by transmitting incoming anisotropic diffuse radiation or emitting when it is thermally inhomogeneous. We present evaluations of instrumental polarization generated by materials usually adopted in Radioastronomy, by using the Mueller matrix formalism. As an application, results for different slabs in front of a 32 GHz receiver are discussed. Such results are based on measurements of their complex dielectric constant. We evaluate that a 0.33 cm thick Teflon slab introduces negligible spurious polarization ($< 2.6 \times 10^{-5}$ in transmission and $< 6 \times 10^{-7}$ in emission), even minimizing the leakage ($< 10^{-8}$ from Q to U Stokes parameters, and viceversa) and the depolarization ($\sim 1.3 \times 10^{-3}$).

OCIS codes: 120.5410, 350.4010, 230.5440, 350.1260, 350.5500.

1. Introduction

The last decade has been characterized by the growing interest into the Cosmic Microwave Background Polarization (CMBP), that has stimulated the design of polarimeters featured by low systematic effects and high sensitivity in microwave frequencies. The CMBP, in fact, is among the most powerful tool to investigate the early stages of the Universe.[1] Due to the faint expected signal (a few μK over the ~ 3 K unpolarized component), any instrumental effect that can produce spurious polarization must be analyzed in detail in order to minimize its impact. Weak signals call for high sensitive radiometers that are usually realized by cooling down the front-end to cryogenic temperatures by means of cryostats. In Radioastronomy, homogeneous and low loss dielectric slabs are used to allow the signal to enter the cryostat (e.g. see experiments in Ref. 2–8). Usually, such materials are considered isotropic and then not generating instrumental polarization. Hence, no analysis is performed to study polarization effects related to isotropic flat dielectrics. This work arises from the need to investigate the linear instrumental polarization introduced by flat vacuum windows in microwave polarimeters when considered isotropic, thus providing the relationship

[1] present address: INAF-IASF Roma, Via del Fosso del Cavaliere 100, 00133 Roma, Italy
[2] present address: INAF-IRA Bologna, Via Gobetti 101, 40129 Bologna, Italy

with the material properties through either the complex dielectric constant or the complex index of refraction. However, the results reported in this paper are not exhaustive as far as the complete design of vacuum windows is concerned. Other effects may occur to enhance the systematics, such as possible intrinsic or manufacturing induced birefringence of the sample,[9] and the present work should be considered as a first attempting to investigate and minimize the spurious instrumental polarization that may arise from flat isotropic dielectric slabs. We find that a uniform diffuse radiation does not generate instrumental polarization, which, instead, is generated by anisotropic components (e.g. CMB). We also estimate the amount of the effects in the specific case of isotropic dielectric which works in Ka frequency band, centered at 32 GHz, an interesting band in microwave cosmology.
The paper is organized as follows: in Section (2) we present the theoretical model used to derive the polarization effects introduced by flat isotropic dielectrics, while in Section (3) we present the total intensity analysis which provides reflectance, transmittance and absorptance of the materials. Measurements of their complex dielectric constants are presented in section (4) and, finally, estimates of the spurious effects predicted by the model for the dielectrics experimentally investigated are reported in section (5).

2. Instrumental polarization by flat isotropic dielectric slab

The instrumental polarization can be evaluated from the Stokes parameter equations:[10]

$$I^x \propto \langle|E_p^x|^2\rangle + \langle|E_t^x|^2\rangle \quad (1)$$

$$Q^x \propto \langle|E_p^x|^2\rangle - \langle|E_t^x|^2\rangle \quad (2)$$

$$U^x \propto \langle 2\Re\{E_p^x E_t^{x^*}\}\rangle \quad (3)$$

$$V^x \propto \langle 2\Im\{E_p^x E_t^{x^*}\}\rangle \quad (4)$$

where E_p^x and E_t^x are the complex parallel and perpendicular components of the electric field with respect to the incident plane, $\langle\rangle$ denotes the time average (henceforth we will omit it for clarity), and $x = R, T$ indicates the reflection and transmission terms, respectively.
The transmission case writes

$$E_j^T = T_j E_j \quad (5)$$

where $j = p, t$ denotes the parallel and perpendicular components of the incoming E_j electric field and T_j is its complex transmission coefficient due to the flat dielectric slab.[11–14] Using Eq. (5) in Eq. (1)–(4), the Stokes parameters of the transmitted wave, computed in the reference frame defined by the plane of incidence, are given by

$$\mathbf{S}^T = \mathbf{M}^T \mathbf{S}^0 \quad (6)$$

where $\mathbf{S}^0 \equiv [I^0, Q^0, U^0, V^0]$ and $\mathbf{S}^T \equiv [I^T, Q^T, U^T, V^T]$ are the Stokes parameters of the incoming and transmitted radiation respectively, and

$$\mathbf{M}^T = \begin{pmatrix} \frac{1}{2}(|T_p|^2 + |T_t|^2) & \frac{1}{2}(|T_p|^2 - |T_t|^2) & 0 & 0 \\ \frac{1}{2}(|T_p|^2 - |T_t|^2) & \frac{1}{2}(|T_p|^2 + |T_t|^2) & 0 & 0 \\ 0 & 0 & \Re\{T_p T_t^*\} & \Im\{T_p T_t^*\} \\ 0 & 0 & -\Im\{T_p T_t^*\} & \Re\{T_p T_t^*\} \end{pmatrix} \tag{7}$$

is the Mueller matrix.[10] Since generally $T_p \neq T_t$ and $T_p T_t^* \neq 0$, a flat isotropic dielectric slab generates cross-contamination between I and Q, and U and V parameters.
An interesting case is that of unpolarized incoming radiation, defined by I^0_{un}. In this case, the outgoing radiation is featured by

$$\mathbf{S}^T = \begin{pmatrix} \frac{1}{2}(|T_p|^2 + |T_t|^2) I^0_{\text{un}} \\ \frac{1}{2}(|T_p|^2 - |T_t|^2) I^0_{\text{un}} \\ 0 \\ 0 \end{pmatrix} \tag{8}$$

Therefore, an instrumental polarization is generated and the contamination affects only Q. Hereafter, we call it *spurious polarization*.
Similar considerations hold for the reflection case, by replacing T_j by R_j.
It is worth noting that $\mathbf{M}^T$ (and $\mathbf{M}^R$) is the product of the Mueller matrices of polarizer and retarder,[10] allowing the description of a flat isotropic dielectric slab as a combination of these two polarizing devices.
About the effects generated by the emitted radiation, we adopt an approach based on the radiation power rather than on the electric field. The signal emitted by the slab is thermal noise characterized by a continuum spectrum related to the physical temperature of the dielectric $\mathrm{T_{ph}}$. In the microwave frequency domain, by adopting the Rayleigh-Jeans approximation, the brightness temperature of a thermal source is proportional to its physical temperature.[15] Thus, the two intensity components (parallel and perpendicular) of the emitted signal can be computed as

$$|E_j^\varepsilon|^2 \propto \varepsilon_j \mathrm{T_{ph}} \tag{9}$$

where ε_j is the Emittance for the j-component. Assuming that the slab is in thermal equilibrium, the equivalence between Emittance ε_j and Absorptance A_j holds[16]

$$\varepsilon_j(\nu, \theta_i) \equiv A_j(\nu, \theta_i) = 1 - |R_j(\nu, \theta_i)|^2 - |T_j(\nu, \theta_i)|^2 \tag{10}$$

allowing us the computation of the emission coefficients from those of reflection and transmission. Due to the thermal noise nature of the emitted components, these can be considered uncorrelated,[16] so that the Stokes parameters write

$$\mathbf{S}^\varepsilon = \begin{pmatrix} \frac{1}{2}(\varepsilon_p + \varepsilon_t)\mathrm{T_{ph}} \\ \frac{1}{2}(\varepsilon_p - \varepsilon_t)\mathrm{T_{ph}} \\ 0 \\ 0 \end{pmatrix} \tag{11}$$

giving the interesting result that the thermal noise injected by the flat slab is partially polarized. Once again, the contamination affects only Q.
In case of unpolarized incoming radiation, it is convenient to describe the instrumental polarization through the equations

$$Q_{SP}^{R} = SP^{R}\, I_{\rm un}^{0} \quad (12)$$
$$Q_{SP}^{T} = SP^{T}\, I_{\rm un}^{0} \quad (13)$$
$$Q_{SP}^{\varepsilon} = SP^{\varepsilon}\, \mathrm{T_{ph}} \quad (14)$$

with the *spurious polarization coefficients* SP given by

$$SP^{R} = \frac{1}{2}(|R_p|^2 - |R_t|^2) \quad (15)$$
$$SP^{T} = \frac{1}{2}(|T_p|^2 - |T_t|^2) \quad (16)$$
$$SP^{\varepsilon} = \frac{1}{2}(\varepsilon_p - \varepsilon_t) \quad (17)$$

While $|R_j|^2$ and $|T_j|^2$ can be measured, it is generally hard to measure ε_j and, in turn, the coefficient SP^{ε}. However, it is straightforward that the relation

$$SP^{R} + SP^{T} + SP^{\varepsilon} = 0 \quad (18)$$

holds, providing thus a way to evaluate SP^{ε}.
Interesting special case is that of perpendicular incident radiation ($\theta_i = 0$ in Fig. 1), for which $|R_p|^2 = |R_t|^2$ and $|T_p|^2 = |T_t|^2$, then

$$SP^{x}(\theta_i = 0) = 0 \quad (19)$$

that is no spurious polarization is generated.
Frequently, the dielectric slab is placed in front of a collecting system (e.g. a feed-horn which we assume aligned with the slab axis), thus it is important to evaluate the instrumental polarization propagating inside the receiver. Contributions come from the radiation transmitted and emitted by the dielectric. In fact, a further signal can be generated by reflection due to the signal emitted by the receiver toward the free space and backscattered by the slab. However, this occurs at angles of incidence $\theta_i \sim 0$, thus implying negligible SP^{R}.
The Eq. (6) and (11) provide the instrumental polarization due to the radiation coming from a given direction and in the reference frame defined by the plane of incidence and its normal (see Fig. 1).
Such signals must be evaluated in the laboratory reference frame (e.g. the Antenna Reference Frame: *ARF*), by accounting for the rotation of the azimuthal angle β. By referring to Fig. 1, if $\mathbf{S}_{\rm ARF}^{0}$ defines the Stokes parameters of the incoming radiation in the *ARF*, the polarization state of the transmitted component can be described as:[10]

$$\mathbf{S}_{\rm ARF}^{T}(2\beta) = \mathbf{R}(-2\beta)\mathbf{M}^{T}\mathbf{R}(2\beta)\, \mathbf{S}_{\rm ARF}^{0} = \mathbf{H}^{T}(2\beta)\, \mathbf{S}_{\rm ARF}^{0} \quad (20)$$

where the $\mathbf{H}^T(2\beta)$ matrix is:

$$\begin{pmatrix} T & SP^T\cos(2\beta) & SP^T\sin(2\beta) & 0 \\ SP^T\cos(2\beta) & T\cos^2(2\beta)+M_{33}^T\sin^2(2\beta) & (T-M_{33}^T)\sin(2\beta)\cos(2\beta) & -L^T\sin(2\beta) \\ SP^T\sin(2\beta) & (T-M_{33}^T)\sin(2\beta)\cos(2\beta) & T\sin^2(2\beta)+M_{33}^T\cos^2(2\beta) & L^T\cos(2\beta) \\ 0 & L^T\sin(2\beta) & -L^T\cos(2\beta) & M_{33}^T \end{pmatrix} \tag{21}$$

and

$$T = \frac{1}{2}(|T_p|^2+|T_t|^2) \tag{22}$$

$$L^T = \Im\{T_pT_t^*\} \tag{23}$$

$$M_{33}^T = \Re\{T_pT_t^*\} \tag{24}$$

where $\mathbf{R}(2\beta)$ is the Mueller matrix for rotation[10] and T is the Transmittance of the slab. Given an input Stokes parameter Y^0, we define its contamination over the X output as $\mathrm{X}_{\mathrm{Y}^0}$: such a cross-term is the *leakage*. Thus, by definition, the transmission function of the X^0 parameter is $\mathrm{X}_{\mathrm{X}^0}$.
About the emitted component, in the *ARF* the signal expected is:

$$\mathbf{S}_{\mathrm{ARF}}^{\varepsilon}(2\beta) = \begin{pmatrix} \varepsilon \mathrm{T_{ph}} \\ SP^{\varepsilon}\cos(2\beta)\mathrm{T_{ph}} \\ SP^{\varepsilon}\sin(2\beta)\mathrm{T_{ph}} \\ 0 \end{pmatrix} \tag{25}$$

where $\varepsilon = \frac{1}{2}(\varepsilon_p+\varepsilon_t)$ is the Emittance of the slab.
It is worth noting that each quantity hitherto discussed is well-defined for values of the polar angle up to $\frac{\pi}{2}$ rad.
The effect on the spurious polarization due to the incoming unpolarized diffuse signal characterized by a brightness temperature distribution[15] $\mathrm{T_b}(\nu,\theta,\beta)$ can be computed by integrating the spurious components (SP^T) of Eq. (20) all over the directions. Such integrations lead to the following outputs for Q and U in antenna temperature:[15]

$$Q_{SP}^T(d) = \frac{1}{\Omega_A^{\mathrm{FF}}\Delta\nu}\int_{\Delta\nu}\left[\int_0^{\pi/2}\mathrm{d}\theta SP^T(d,\nu,\theta\,')P_n^{\mathrm{FF}}(\theta)\sin(\theta)\int_0^{2\pi}\mathrm{d}\beta \mathrm{T_b}(\nu,\theta,\beta)\cos(2\beta)\right]\mathrm{d}\nu \tag{26}$$

$$U_{SP}^T(d) = \frac{1}{\Omega_A^{\mathrm{FF}}\Delta\nu}\int_{\Delta\nu}\left[\int_0^{\pi/2}\mathrm{d}\theta SP^T(d,\nu,\theta\,')P_n^{\mathrm{FF}}(\theta)\sin(\theta)\int_0^{2\pi}\mathrm{d}\beta \mathrm{T_b}(\nu,\theta,\beta)\sin(2\beta)\right]\mathrm{d}\nu \tag{27}$$

where $\Delta\nu$ is the frequency bandwidth, P_n^{FF} and Ω_A^{FF} are the normalized co-polar pattern and the antenna solid angle in far field regime[15] respectively; $\theta\,'(\theta)$ is the angle of incidence on the slab of the radiation coming from the (far field) direction θ: if the slab is in the near field of the antenna, then $\theta\,' < \theta$ (flat slab and antenna are assumed coaxial, so $\theta_i \equiv \theta$), otherwise in far field $\theta\,' \equiv \theta$. In order to emphasize the effect introduced by the slab, in Eq. (26) and (27) we assume an ideal feed-horn featured by a β-symmetric co-polar pattern (i.e. null cross-polarization), the feed horn

spectral transfer function constant all over the frequency band ($P_n(\nu,\theta,\beta) \equiv P_n(\theta)$) and negligible edge effects between the slab and the feed aperture in the case of near field position.
Writing the brightness temperature with respect to its mean and anisotropy components

$$\mathrm{T_b}(\nu,\theta,\beta) = \mathrm{T_{b,0}}(\nu) + \Delta\mathrm{T_b}(\nu,\theta,\beta) \tag{28}$$

makes null the contribution of the mean term in the Eq. (26)–(27), which thus become

$$Q^T_{SP}(d) = \frac{1}{\Omega^{\mathrm{FF}}_A \Delta\nu} \int_{\Delta\nu} \mathrm{d}\nu \int_0^{\pi/2} \mathrm{d}\theta SP^T(\theta\,') P^{\mathrm{FF}}_n(\theta) \sin(\theta) \int_0^{2\pi} \mathrm{d}\beta \Delta\mathrm{T_b}(\nu,\theta,\beta) \cos(2\beta) \tag{29}$$

$$U^T_{SP}(d) = \frac{1}{\Omega^{\mathrm{FF}}_A \Delta\nu} \int_{\Delta\nu} \mathrm{d}\nu \int_0^{\pi/2} \mathrm{d}\theta SP^T(\theta\,') P^{\mathrm{FF}}_n(\theta) \sin(\theta) \int_0^{2\pi} \mathrm{d}\beta \Delta\mathrm{T_b}(\nu,\theta,\beta) \sin(2\beta) \tag{30}$$

This gives the important result that a flat isotropic dielectric slab can generate spurious polarization only in presence of anisotropic incoming signal. Similarly, in axisymmetric optics[17,18] the instrumental polarization is generated only by incoming anisotropic radiation. This is particularly relevant for the CMB, whose anisotropy is low ($\Delta\mathrm{T_b}/\mathrm{T_b} \sim 10^{-5}$).[19,20]
The spurious polarization due to the emission, can be computed by replacing $\mathrm{T_b}$ with the physical temperature and, from Eq. (25), the correlated component of the thermal noise collected by the feed is

$$Q^\varepsilon_{SP}(d) = \frac{1}{\Omega^{\mathrm{NF}}_A \Delta\nu} \int_{\Delta\nu} \mathrm{d}\nu \int_0^{\pi/2} \mathrm{d}\theta SP^\varepsilon(d,\nu,\theta) P^{\mathrm{NF}}_n(\theta) \sin(\theta) \int_0^{2\pi} \mathrm{d}\beta\ \Delta\mathrm{T_{ph}}(\theta,\beta) \cos(2\beta) \tag{31}$$

$$U^\varepsilon_{SP}(d) = \frac{1}{\Omega^{\mathrm{NF}}_A \Delta\nu} \int_{\Delta\nu} \mathrm{d}\nu \int_0^{\pi/2} \mathrm{d}\theta SP^\varepsilon(d,\nu,\theta) P^{\mathrm{NF}}_n(\theta) \sin(\theta) \int_0^{2\pi} \mathrm{d}\beta\ \Delta\mathrm{T_{ph}}(\theta,\beta) \sin(2\beta) \tag{32}$$

where P^{NF}_n is the normalized co-polar pattern in near field at the slab position if it is placed in the near field of the antenna. Even in this case, the contribution of the mean component is null and the spurious polarization equations are like for Eq. (29)–(30), but with the anisotropic thermal component $\Delta\mathrm{T_{ph}}$ instead of $\Delta\mathrm{T_b}$, and P^{FF}_n replaced by P^{NF}_n.
Since both the transmitted and emitted signals are not correlated, due to the additive property of the Stokes parameters[10] the total spurious polarizations is

$$Q_{SP} = Q^T_{SP} + Q^\varepsilon_{SP} \tag{33}$$

$$U_{SP} = U^T_{SP} + U^\varepsilon_{SP} \tag{34}$$

From the matrix $\mathbf{H}^T(2\beta)$, the depolarization of Q and U can be estimated as:

$$D_{Q^T} = \frac{Q^0 - Q^T}{Q^0} = (1-T)\cos^2(2\beta) + (1-M^T_{33})\sin^2(2\beta) \tag{35}$$

$$D_{U^T} = \frac{U^0 - U^T}{U^0} = (1-T)\sin^2(2\beta) + (1-M^T_{33})\cos^2(2\beta) \tag{36}$$

The loss of the Q-signal, D_{Q^T}, could be evaluated in percentage term with respect to the measured Q_m^0 in absence of the slab. The result is:

$$\eta_{Q^T}(d) = \frac{\frac{1}{\Omega_A^{\rm FF}\Delta\nu}\int_{\Delta\nu}{\rm d}\nu\int_0^{\pi/2}{\rm d}\theta\ {\rm P_n^{FF}}(\theta)\sin(\theta)\int_0^{2\pi}{\rm d}\beta\ {\rm D_{Q^T}(d,\nu,\theta\,',\beta)Q^0(\nu,\theta,\beta)}}{\frac{1}{\Omega_A^{\rm FF}\Delta\nu}\int_{\Delta\nu}{\rm d}\nu\int_0^{\pi/2}{\rm d}\theta\ {\rm P_n^{FF}}(\theta)\sin(\theta)\ \int_0^{2\pi}{\rm d}\beta{\rm Q^0(\nu,\theta,\beta)}} \quad (37)$$

The same for U. Assuming a constant incoming signal ($Q^0(\nu,\theta,\beta) = Q^0$), a zero-order estimate of Eq. (37) is given by:

$$\begin{aligned}\eta_{Q^T}(d) &= \frac{2\pi}{\Omega_A^{\rm FF}}\int_0^{\pi/2}\tilde{D}_{Q^T}(d,\theta\,')P_n^{FF}(\theta)\sin(\theta)\ {\rm d}\theta \quad (38)\\ \tilde{D}_{Q^T}(d,\theta\,') &= \frac{1}{2\pi}\int_0^{2\pi}\langle D_{Q^T}(d,\nu,\theta\,',\beta)\rangle_\nu\ {\rm d}\beta = \\ &= \frac{1}{2}\left[1-\langle T(d,\nu,\theta\,')\rangle_\nu + 1 - \langle M_{33}^T(d,\nu,\theta\,')\rangle_\nu\right] \quad (39)\end{aligned}$$

where $\langle\rangle_\nu$ is the in-band average.
The $Q_{U^0}^T$ leakage term results:

$$\begin{aligned}Q_{U^0}^T(d) = \frac{1}{\Omega_A^{\rm FF}\Delta\nu}\int_{\Delta\nu}{\rm d}\nu\int_0^{\pi/2}{\rm d}\theta\ \left[{\rm T(d,\nu,\theta\,') - M_{33}^T(d,\nu,\theta\,')}\right]{\rm P_n^{FF}}(\theta)\sin(\theta)\\ \times\int_0^{2\pi}{\rm d}\beta\ \sin(2\beta)\cos(2\beta){\rm \Delta U^0(\nu,\theta,\beta)} \quad (40)\end{aligned}$$

The same for $U_{Q^0}^T$ by replacing Q with U. Note that a non null result arises if the incoming signal is anisotropic.
Finally, the leakage due to V^0 is given by:

$$Q_{V^0}^T(d) = -\frac{1}{\Omega_A^{\rm FF}\Delta\nu}\int_{\Delta\nu}{\rm d}\nu\int_0^{\pi/2}{\rm d}\theta{\rm L^T(d,\nu,\theta\,')P_n^{FF}}(\theta)\sin(\theta)\int_0^{2\pi}{\rm d}\beta\ \sin(2\beta){\rm \Delta V^0(\nu,\theta,\beta)} \quad (41)$$

$$U_{V^0}^T(d) = \frac{1}{\Omega_A^{\rm FF}\Delta\nu}\int_{\Delta\nu}{\rm d}\nu\int_0^{\pi/2}{\rm d}\theta{\rm L^T(d,\nu,\theta\,')P_n^{FF}}(\theta)\sin(\theta)\int_0^{2\pi}{\rm d}\beta\ \cos(2\beta){\rm \Delta V^0(\nu,\theta,\beta)} \quad (42)$$

Once again, a leakage is generated only in case of anisotropic incoming signal.

3. Total intensity analysis

The effects on the total intensity signal can be evaluated by estimating both transmission and reflection properties of the slab (see for details Ref. 11–14).
The incoming signal collected by the system slab-feed is given by (in antenna temperature):

$${\rm T_A^T}(d) = \frac{1}{\Omega_A^{\rm FF}\Delta\nu}\int_0^{\pi/2}{\rm d}\theta\int_0^{2\pi}{\rm d}\beta\int_{\Delta\nu}{\rm d}\nu\ T(d,\nu,\theta\,'){\rm T_b}(\nu,\theta,\beta)\ P_n^{\rm FF}(\theta)\sin(\theta) \quad (43)$$

where T is the Transmittance of the slab.
An estimate of the effect is given by the relative transmitted signal $\Lambda(d) = \mathrm{T}_A^T(d)/\mathrm{T}_0$ in the simple case of an isotropic input signal $\mathrm{T_b}(\nu, \theta, \beta) = \mathrm{T}_0$:

$$\Lambda(d) = \frac{2\pi}{\Omega_A^{\mathrm{FF}}} \int_0^{\pi/2} \langle T(d, \nu, \theta\,') \rangle_\nu P_n^{\mathrm{FF}}(\theta) \sin(\theta) \mathrm{d}\theta \tag{44}$$

If the feed horn directivity is high, most of the signal is collected close to 0°. In the limit of low loss dielectrics, the maxima of $\Lambda(d)$ will be identified by integer multiples of the well known thickness $d = d_0 \equiv \lambda/2n$, which identifies the Transmittance maxima for null incidence,[11] where n is the real part of the complex index of refraction.
Similarly, the thermal noise injected by the dielectric can be computed when it is in thermal equilibrium at the physical temperature $\mathrm{T_{ph}}$. Its emission is that of a greybody at temperature $\mathrm{T_{ph}}$ featured by an Emittance $\varepsilon(\theta_i) \equiv A(\theta_i) = 1 - [R(\theta_i) + T(\theta_i)]$, where $R = \frac{1}{2}(|R_p|^2 + |R_t|^2)$ is the Reflectance of the slab. Since here we consider the microwave frequency domain, the Rayleigh-Jeans approximation can be adopted. Hence, in term of brightness temperature,[15] the thermal noise emitted by the slab is simply $\varepsilon(\theta_i)\mathrm{T_{ph}}$. Thus, the signal collected by the antenna is:

$$\mathrm{T}_A^\varepsilon(d) = \frac{1}{\Omega_A^{\mathrm{NF}} \Delta\nu} \int_0^{\pi/2} \mathrm{d}\theta \int_0^{2\pi} \mathrm{d}\beta \int_{\Delta\nu} \mathrm{d}\nu\ \varepsilon(d, \nu, \theta)\ \mathrm{T_{ph}}(\theta, \beta) P_n^{\mathrm{NF}}(\theta) \sin(\theta) \tag{45}$$

where $P_n^{\mathrm{NF}}(\theta)$ is the Near Field normalized co-polar pattern of the feed if the slab is placed at its near field, and a thermally inhomogeneous but thermally stabilized slab has been considered.
In a conservative approach, the antenna noise temperature can be estimated as:

$$\mathrm{T}_A^\varepsilon(d) \leq \langle \varepsilon(d, \nu, \theta) \rangle_\nu |_{\mathrm{MAX}(\theta)} \times \mathrm{T_{ph}}(\theta, \beta)|_{\mathrm{MAX}(\theta,\beta)} \tag{46}$$

where $\mathrm{MAX}(y)$ stands for the maximum value over the quantity y.

4. Microwave Tests

In order to provide realistic estimates of the analysis hitherto carried out, we performed measurements on several samples to determine their complex dielectric constant ϵ ($\epsilon = \epsilon_r[1 - i\tan(\delta_e)]$, where $\tan(\delta_e)$ is the electric tangent loss), which entries in the determination of the R_j, T_j and ε_j quantities[11–14] by means of the complex index of refraction $\mathbf{n}$ ($\mathbf{n} = n - i\kappa$, where κ is the extinction coefficient). In fact, they are related as follow (for $\mu_r = 1$):

$$n = \sqrt{\frac{\epsilon_r}{2}} \left[\sqrt{1 + \tan^2(\delta_e)} + 1 \right]^{1/2} \Big|_{\tan(\delta_e) << 1} \simeq \sqrt{\epsilon_r} \tag{47}$$

$$\kappa = \sqrt{\frac{\epsilon_r}{2}} \left[\sqrt{1 + \tan^2(\delta_e)} - 1 \right]^{1/2} \Big|_{\tan(\delta_e) << 1} \simeq \frac{1}{2}\sqrt{\epsilon_r} \tan(\delta_e) \tag{48}$$

Since electromagnetic properties of polymers can vary with the composition, history and temperature of the specimen,[21] measurements are mandatory. As a matter of

fact, it is convenient to extract the slab of interest from the same bulk of material used to cut the samples under test.
We have investigated High Density Polyethylene (HDPE), Teflon, Polypropylene and Nylon, which are dielectrics commonly used from microwave to far infrared frequencies. The tests have been performed in the frequency band $27 < \nu < 37$ GHz, interesting for microwave cosmology.[22] The measurements have been performed by means of a vector network analyzer (Model HP8510). A waveguide device has been realized in standard WR-28. It consists of two shells cut along the E-plane (Fig. (2)) which embeds the test sample. The test is based on the comparison of the reflection and transmission parameters S_{11} and S_{21} of the global device[23] (waveguide plus sample), by making two measurements with and without the dielectric test sample. The measured insertion loss and return loss can be related to impedance and propagation constants characterizing the equivalent transmission line of the fundamental mode. In turn, these constants are related to ϵ_r (one of the wanted quantity), the resistivity of the material ρ_m and the size of the sample, so allowing the computation of the other relevant quantity, $\tan(\delta_e)$. Estimates of ϵ_r and $\tan(\delta_e)$ are carried out by performing a best fit on the data and assuming a second order polynomial behavior for ϵ_r and ρ_m. Such estimates will be specialized by computing their in-band (30.4–33.6 GHz) average values, which are those of interest to the BaR-SPOrt project. An example of our results is reported in Fig. (3), which shows the measurements and the best fit model of the scattering parameters in the case of a Teflon sample. The main error source for the fitting procedure comes from the knowledge of the sample sizes (reported in Table (1); see also Fig. (4) for parameter definitions). Such errors are taken into account when computing the in-band average values. In Fig. (5) the complex constants are shown while Table (2) and (3) report the in–band average values and variations. For sake of completeness, we compare our data with those reported in the literature (see Table (4)). There is a good consistency for the estimated dielectric constants. Large differences, instead, are found for the electric tangent loss of Teflon and Polypropylene. The poor precision is due to the experimental technique adopted, which is not ideal for low loss dielectrics. In this case, a more accurate evaluation of the electric tangent loss could be obtained by applying the cavity technique.[25] These considerations look supported by the high precision data of both ϵ_r and $\tan(\delta_e)$ obtained for the Nylon sample. Although we provide just upper limits for $\tan(\delta_e)$, no higher precision measurements seem necessary since the contamination computed in Section (5) are already negligible. Due to our interest in tiny polarization signal, we performed extensive measurements on Teflon to investigate its optical anisotropy. In fact, it seems to be more promising among the materials selected. The manufacturing, in fact, can introduce in these polymers anisotropic electromagnetic and structural properties, since the molecular chains (structural units) will be preferentially aligned in certain directions,[26,27] thus transforming the dielectric into a sort of polarizer. Hence, we preferred to use a Teflon block that has been casted and not extruded to minimize such manufacturing effects. We assume such a block as homogeneous. By considering the vibration of the electric field propagating in the rectangular waveguide, it is possible to investigate the optical anisotropy of dielectrics by cutting the sample as shown in Fig (4). Since typical feeds for microwave cosmology are charac-

terized by high directivity,[4,28,29] most of the signal will be collected close to 0°. Thus, two samples have been cut along the z–axis, but rotated by 90° each other, to probe the material for the incoming electric field vibrating in x and y directions.
The results in the two directions are consistent each other within the error (see Fig. (6) and Table (5)), and possible anisotropy of the complex index of refraction between 0° and 90° of rotation is summarized by the following data:

$$\Delta\langle n\rangle_\nu = \langle n\rangle_\nu^{1-\mathrm{cut}} - \langle n\rangle_\nu^{2-\mathrm{cut}} = 0.01 \pm 0.01 \quad (49)$$

$$\Delta\langle \kappa\rangle_\nu = \langle \kappa\rangle_\nu^{1-\mathrm{cut}} - \langle \kappa\rangle_\nu^{2-\mathrm{cut}} = (4.2 \pm 5.8) \times 10^{-5} \quad (50)$$

which means that we can set at 1σ of Confidence Level the following upper limit: $\overline{\Delta\langle n\rangle_\nu} = 0.02$ and $\overline{\Delta\langle \kappa\rangle_\nu} = 10^{-4}$. These measurements allow us to consider our Teflon sample optically isotropic at least for our purposes.

5. Estimates of the systematic effects.

The analysis performed in Section (2) includes the far and near field regime, even though for our purpose most estimates will be provided for a flat slab placed in near field position. However one case of far field will be also considered. We take into account an instrument featured by a 10% bandwidth, typical of recent microwave polarimeters, so that all the relevant quantities of Sections (2) and (3) are evaluated as in-band average. Furthermore, here we replace the angle θ' with θ (i.e. the incoming Far Field direction) making easier the computation of all the interesting quantities. This approximation does not prevent the aim of this work. In fact, if the slab is close to the feed aperture then $\theta' < \theta$, and, in turn, this substitution provides conservative estimates. The materials considered here are Teflon, HDPE and Polypropylene, disregarding the Nylon due to its high values of ϵ_r and $\tan(\delta_e)$, since we are interested in the minimization analysis of the systematic effects. For the Teflon, we take into account the 1–cut, since its complex index of refraction is more precise than the other cut.
In Fig. (7) the in-band average reflectance, transmittance and emittance of the dielectrics versus θ_i are shown for 3 thickness values. For each panel the central value is the thickness which maximizes the transmission at $\theta_i = 0$ (see the Teflon plots): it corresponds to $d = d_0 \equiv \lambda/2n$ where $\lambda \sim 0.94$ cm. As expected, these plots show that either increasing κ or the thickness generates an increase of the emittance. Similarly, the reflectance increases by increasing n. Close to the axis, transmittance variations are very small (for $\theta_i < 15°$ is lower than 10^{-3}), then $T(d, \nu, \theta') \simeq T(d, \nu, \theta)$, so allowing the substitution θ' with θ. In these frequencies such dielectrics show very low losses ($\sim 10^{-3} \div 10^{-4}$, see the emittance plot), then the thickness d_0 provides a good estimate of the thickness that maximizes the transmittance.
A first estimate of the thermal noise ($\mathrm{T_{noise}}$) injected by the slab can be given by Eq. (46) using the parameter $\langle\varepsilon(d, \nu, \theta)\rangle_\nu|_{\mathrm{MAX}(\theta)}$ (see bottom-right plot of Fig. (7) and Table (6) for the estimates).
A better estimate of the signal transmission and of the thermal noise collected by the feed (Fig. (8)) can be given using Eq. (44) and (45) where, for the emission, the near field pattern has to be used. The adopted patterns are shown in Fig. (9), by using the

BaR-SPOrt far field one as realistic example,[29] and by assuming a Gaussian beam approximation for the near field.[31] In the last case, it is necessary to set a geometrical configuration of the slab in front of the feed aperture to produce the near field pattern. Then, for our purpose, a circular flat slab will be adopted. Hereafter, we will refer to the estimates of quantities related to antenna integrals as "BaR-SPOrt case" but, as we will show in this section, the core idea can be applicable in the same way to other cases. The plot in Fig. (8) shows, as expected, that the noise due to the slab increases with the thickness. The plot of the relative transmitted signal Λ shows the typical interference trend. As highlighted in the magnified frame, the value of the first maximum correspond to a thickness of 0.33 cm for the Teflon and 0.31 cm for HDPE and Polypropylene, that is the ideal value d_0 in case of the low absorbing material approximation. It is due to the narrow beam of the feed adopted which favors angles very close to 0°. Thus, in case of narrow far field pattern, such a thickness provides the best size for maximizing the transmittance of the slab. By choosing as optimal thickness d_0, the residuals with respect to 1 (i.e. $\Lambda(d) - 1$) give an estimate of the signal loss ($\sim 10^{-3}$). Besides the slab thickness optimization, this analysis allows us to choose even the best material, which in the band adopted is Teflon.
Table (6) shows the parameters $\langle \varepsilon(d,\nu,\theta)\rangle_\nu|_{\mathrm{MAX}(\theta)}$ and the quantity $\mathrm{T}_A^\varepsilon(d)/\mathrm{T}_{\mathrm{ph}}^{\mathrm{MAX}}$ obtained by increasing the antenna integral in Eq. (45) that are used to evaluate the noise temperature injected by the slab ($\mathrm{T}_{\mathrm{noise}}$). Between the two estimates, the beam integration gives a correction of $\sim 10\%$ reducing the value provided by the Eq. (46): the estimates are the same within 10% variation. Thus, the Eq. (46) is an easy way to estimate the thermal noise. As shown, the Teflon is the material which injects the lowest noise (162 mK at $\mathrm{T}_{\mathrm{ph}}^{\mathrm{MAX}} = 300$ K), even though HDPE is just slightly worst and can be considered as well.
The spurious polarization coefficients are shown in Fig. (10). Oscillations in the spurious response are generated by increasing the optical path inside the slab as is typical for interference phenomena. Once again, the approximation for the angle can be applied since, close to the feed axis, the relation $|\langle SP^T(d,\nu,\theta')\rangle_\nu| < |\langle SP^T(d,\nu,\theta)\rangle_\nu|$ holds. Then a conservative estimate of Eq. (29)–(32) can be represented by:

$$Q_{SP}^x|_{\mathrm{MAX}} = U_{SP}^x|_{\mathrm{MAX}} = |\langle SP^x(d,\nu,\theta)\rangle_\nu|_{\mathrm{MAX}(\theta)} \times |\Delta\mathrm{T}(\nu,\theta,\beta)|_{\mathrm{MAX}(\nu,\theta,\beta)} \tag{51}$$

where x is either T or ε, and ΔT is the variation of either the brightness or the physical temperature.
The upper limit of the spurious polarized transmission and emission are plotted in Fig. (11) for the BaR-SPOrt case by conservatively approximating the Eq. (29) as follows:

$$\begin{aligned} Q_{SP}^T(d) = & \frac{1}{\Omega_A^{\mathrm{FF}}\Delta\nu}\int_{\Delta\nu}\mathrm{d}\nu\int_0^{\pi/2}\mathrm{d}\theta SP^T(d,\nu,\theta')P_n^{\mathrm{FF}}(\theta)\sin(\theta)\times \\ & \times\int_0^{2\pi}\mathrm{d}\beta\Delta\mathrm{T_b}(\nu,\theta,\beta)\cos(2\beta) \qquad (52) \\ & < |\Delta\mathrm{T_b}(\nu,\theta,\beta)|_{\mathrm{MAX}}\ \frac{2\pi}{\Omega_A^{\mathrm{FF}}}\int_0^{\pi/2}|\langle SP^T(d,\nu,\theta)\rangle_\nu|P_n^{\mathrm{FF}}(\theta)\sin(\theta)\ \mathrm{d}\theta \qquad (53) \end{aligned}$$

while the Eq. (31), computed in cylindrical coordinates, has been approximated as:

$$Q^{\varepsilon}_{\mathrm{SP}}(d,z) < \Delta \mathrm{T}_{\mathrm{ph}}(\nu,\rho,\beta)|_{\mathrm{MAX}} \ \frac{2\pi}{\Omega^{\mathrm{NF}}_{A}} \int_{0}^{R} \ |\langle SP^{\varepsilon}(d,\nu,\rho)\rangle_{\nu}| \ P^{\mathrm{NF}}_{n}(\rho,z) \ \ \rho \ \mathrm{d}\rho \qquad (54)$$

where R is the radius of the circular slab and z its position with respect to the feed horn waist. Such plots show that the low relative spurious polarization of the transmitted component ($10^{-3} \div 10^{-5}$) is minimized by the same thickness d_0 which maximizes the transmittance. For the emitted component, the integrated spurious term is very low ($10^{-6} \div 10^{-8}$).
Once again, it could be useful to compare the two methods to evaluate the spurious polarization. The first one is defined by the Eq. (51), while the second one by Eq. (53) and (54), which even accounts for the antenna pattern. Results, shown in Tables (7) and (8), are computed by taking into account as example the known anisotropic signal of the CMB ($\Delta \mathrm{T}^{\mathrm{MAX}}_{\mathrm{b}} = 100\mu\mathrm{K}$) and a guess value of $\Delta \mathrm{T}^{\mathrm{MAX}}_{\mathrm{ph}} = 1$ K related to the thermal gradient of the slab.
Taking into account the antenna pattern, in the BaR-SPOrt case such values are ~ 200 times lower than the rough estimate provided by the Eq. (51), showing how critical it is to consider the antenna pattern in this case. This is due to the high directivity of the feed horn adopted and to the rapid decrease of the $|SP|$ functions close to 0°. Teflon is the material which introduces the lowest spurious polarizations ($\sim 0.6\mu\mathrm{K}$).
For sake of completeness, we insert an analysis of the spurious polarization generated in transmission regime as the beam of the collecting system increases (Fig. (12)) when the slab is placed in far field (i.e. $\theta' \equiv \theta$). Here a Gaussian pattern has been considered, thus performing a general but optimistic analysis, since in case of co-polar pattern of real feed the expected spurious signal is greater than the level generated by a Gaussian one. In fact, the Gaussian pattern shows a rapid decrease out of the beam, thus producing lowest response as shown for comparison between the minima of Teflon at 7° in the left-plot of Fig. (12) and in Fig. (11) (the difference is a factor 3, ~ 5 dB). The plots in Fig. (12) show that the broader the beam the higher the spurious level generated by the slab. As expected, this is due to the rapid increase of the spurious coefficient $|SP^{T}|$ out of the null incidence (see Fig. (10)). Moreover, the thickness setting positions of minima varies with the beam due to the low directivity of the collecting system as the beam increases. In particular, such positions are different from those expected for narrow beam around null incidence (e.g. see the vertical lines across the left-plot of Fig. (12) and Section (3)). For comparison, the level of spurious effects produced by a good feed featured by low cross-polarization (e.g. - 40 dB of BaR-SPOrt[17,18]), even though not optimised to minimize such a systematic, is $\sim$ - 25 dB, as represented by the horizontal line traced across the right-plot of Fig. (12). Such a level matches the requirements for CMBP experiments. The systematics generated by flat dielectric slabs prevail on that produced by good feeds for beams greater than $\sim 15^{\circ}$, thus requiring either thickness optimization analysis or the choice survey to control spurious polarizations.
The estimates of the depolarization effects introduced by the dielectrics are shown in Fig. (13).

Close to the axis we find that $\langle \tilde{D}_Q^T(d,\nu,\theta\,')\rangle_\nu \sim \langle \tilde{D}_Q^T(d,\nu,\theta)\rangle_\nu$, then it is possible to estimate Eq. (38) approximating $\langle \tilde{D}_Q^T(d,\nu,\theta\,')\rangle_\nu$ with $\langle \tilde{D}_Q^T(d,\nu,\theta)\rangle_\nu$. Thanks to the selected thickness and materials, the loss of the polarized signal is marginal ($\sim 10^{-3}$). It is worth noting that the thickness d_0 maximizing the transmittance also minimizes the depolarization (see the magnified frame of right panel in Fig. (13)).
Finally, the leakages are estimated. In a conservative approach, the $Q_{U^0}^T$ leakage term (Eq. (40)) can be estimated as:

$$Q_{U^0}^T(d) < |\Delta \mathrm{U}^0(\nu,\theta,\beta)|_{\mathrm{MAX}(\nu,\theta,\beta)} \times f_{T,M_{33}^T}(d) \quad (55)$$

$$f_{T,M_{33}^T}(d) = \frac{2\pi}{\Omega_A^{\mathrm{FF}}} \int_0^{\pi/2} [\langle T(d,\nu,\theta)\rangle_\nu - \langle M_{33}^T(d,\nu,\theta)\rangle_\nu]\; P_n^{\mathrm{FF}}(\theta)\sin(\theta)\;\mathrm{d}\theta \quad (56)$$

The approximation holds because the term $(\langle T\rangle_\nu - \langle M_{33}^T\rangle_\nu)$ has a monotone growing trend for θ_i comparable with the BaR-SPOrt beam ($\sim 7^\circ$), as shown in top-left panel of Fig. (14). For the selected thickness and materials, the maximum leakage from U^0 to Q in the 30.4–33.6 GHz band is about $0.07\times|\Delta U^0|_{\mathrm{MAX}}$. A more rigorous computation, which takes into account the beam pattern, provides the result shown in Fig. (14) (bottom-left panel). The minimum leakage is realized with the thickness d_0 for which the values drop down to negligible values ($10^{-8} \div 10^{-9}$ with respect to $|\Delta U^0|_{\mathrm{MAX}}$). Same results hold also for $U_{Q^0}^T$.
Similarly, the $Q_{V^0}^T$ term (Eq. (41)) can be estimated as:

$$Q_{V^0}^T(d) < |\Delta \mathrm{V}^0(\nu,\theta,\beta)|_{\mathrm{MAX}(\nu,\theta,\beta)} \times f_{L^T}(d) \quad (57)$$

$$f_{L^T}(d) = \frac{2\pi}{\Omega_A^{\mathrm{FF}}} \int_0^{\pi/2} \langle |L^T(d,\nu,\theta)|\rangle_\nu\; P_n^{\mathrm{FF}}(\theta)\sin(\theta)\;\mathrm{d}\theta \quad (58)$$

where the considerations done for $(\langle T\rangle_\nu - \langle M_{33}^T\rangle_\nu)$ can be extended to $\langle |L^T|\rangle_\nu$. Teflon, HDPE and Polypropylene introduce in the 30.4–33.6 GHz band a 0.16 maximum leakage of V^0 into Q and U. If such a function is smoothed by the beam pattern, then, for the selected thickness d_0 which also here minimize the effect, the leakage becomes negligible ($10^{-4} \div 10^{-5}$ with respect to $|\Delta \mathrm{V}^0|_{\mathrm{MAX}}$).
Again, among the selected materials, Teflon introduces the lowest leakage and depolarization effects.
Note that the depolarization and leakage in transmission are signal losses which can be recovered by an overall instrument calibration.

6. Conclusion

In this work we presented the systematic effects introduced by a flat slab of isotropic dielectric.
We presented an overall analysis of the interaction between electromagnetic radiation and isotropic dielectric at microwave frequencies, by analyzing transmittance, reflectance, absorptance, spurious polarization, leakage and depolarization by means of the Mueller formalism.
The important result is that spurious polarization, and leakage between the Stokes parameters are produced even by optically isotropic dielectrics, but only when they

are thermally inhomogeneous or the incident radiation is anisotropic. In particular, it has been provided an estimate of the expected systematic effects introduced by Teflon, Polypropylene and HDPE, together with algorithms for their thickness optimization to minimize the effects.
Measurements of dielectric constant and electric tangent loss of Teflon, HDPE, Polypropylene and Nylon have been provided between 27 GHz and 37 GHz at 300 K of physical temperature. The Teflon sample analyzed is featured by the lowest $\langle \epsilon_r \rangle_\nu \sim 2.04$ and $\langle \tan(\delta_e) \rangle_\nu \sim 1.6 \times 10^{-4}$ averaged in the 30.4–33.6 GHz band. Moreover, we found that no optical anisotropy at level of 1% has been measured from our Teflon sample about the index of refraction.
The analysis shows that Teflon, among the selected materials, is the best material in the investigated band which minimizes the systematic effects.
As discussed in Section (5), the optimal thickness to maximize transmission (~ 0.999) and reduce emission (~ 0.00054) is $d = 0.33$ cm. The maximum thermal noise introduced by this slab is 162 mK at a physical temperature of $T_{ph} = 300$ K. This thickness, which minimizes also the transmitted spurious polarization ($< 2.6 \times 10^{-5}$, thus producing in emission a spurious level $< 6 \times 10^{-7}$), the leakage ($< 10^{-8}$ from Q^0 to U, or U^0 to Q, $\sim 5 \times 10^{-5}$ from V^0 to Q or U) and the depolarization ($\sim 1.3 \times 10^{-3}$), corresponds to $d = \lambda/2n$. Broadly speaking, in the approximation of low absorbing material and high feed horn directivity, such a thickness maximizes the transmission and reduces all the other effects.
We have also shown that for dielectrics in far field regime, the transmitted spurious polarization prevails on the one produced by good feeds (cross-polarization ~ -40 dB) for beams greater than $\sim 15°$, thus showing the need of either thickness optimization analysis or the choice survey of flat dielectrics to control spurious polarizations. The position of such thicknesses, which set maxima and minima of the spurious response, depends on the beam adopted.

Acknowledgments

Authors wish to thanks Renzo Nesti and Vincenzo Natale for useful discussion, and the anonymous referee for the useful comments and the encouragement to improve the paper. This work is inserted in the BaR-SPOrt program, an experiment aimed at detecting the CMBP, which is funded by ASI (Italian Space Agency).

References

1. Angelica de Oliveira-Costa, "The Cosmic Microwave Background and Its Polarization", in *Astronomical Polarimetry - Current Status and Future Directions.* ASP proceedings Series. Hawaii, USA, March 15-19, (2004).
   The goal of this review is to provide the state-of-the-art of the CMB polarization from a practical point of view, connecting real-world data to physical models.
2. S. Cortiglioni, G. Bernardi, E. Carretti, S. Cecchini, C. Macculi, C. Sbarra, G. Ventura, M. Baralis, O. Peverini, R. Tascone, S. Bonometto, L. Colombo, G. Sironi, M. Zannoni, V. Natale, R. Nesti, R. Fabbri, J. Monari, M. Poloni, S. Poppi, L. Nicastro, A. Boscaleri, P. de Bernardis, S. Masi, M.V. Sazhin, E.N.

Vinyajkin,"BaR-SPOrt: an experiment to measure the linearly polarized sky emission from both the cosmic microwave background and foregrounds", in *16th ESA Symposium on European Rocket and Balloon Programmes and Related Research*. Edited by Barbara Warmbein, **ESA SP-530**, 271-277, (2003).
In this proceeding the BaR-SPOrt experiment is shown as far as the scientific and technological point of view are concerned.

3. M. Zannoni, C. Macculi, E. Carretti, S. Cortiglioni, G. Ventura, J. Monari, M. Poloni, S. Poppi, "Thermal design and performance evaluation of the BaR–SPOrt cryostat", in *Astronomical Telescopes and Instrumentation*. Edited by J. Antebi, D. Lemke. Proc. SPIE , **5498**, 735–743, (2004).
The goal of this proceeding is to discuss in detail both the thermal design of the cryostat housing the instrument and the preliminary test.
4. B. Keating, P. Timbie, A. Polnarev, J. Steinberger, "Large Angular Scale Polarization of the Cosmic Microwave Background Radiation and the Feasibility of Its Detection", Astrophys. J. **495**, 580–596, (1998).
5. B. Keating, P. Ade, J. Bock, E. Hivon, W. Holzapfel, A. Lange, H. Nguyen, Ki W. Yoon, "BICEP: A Large Angular Scale CMB Polarimeter", in *Polarimetry in Astronomy*. Edited by Silvano Fineschi. Proc. SPIE , **4843**, 284–295, (2003).
This proceeding reports both the design and expected performances of BICEP, a millimeter wave receiver (bolometer-based) designed to measure the polarization of the cosmic microwave background.
6. P. Farese, G. Dall'Oglio, J. Gundersen, B. Keating, S. Klawikowski, L. Knox, A. Levy, P. Lubin, C. O'Dell, A. Peel, L. Piccirillo, J. Ruhl, P. Timbie, "COMPASS: An Upper Limit on Cosmic Microwave Background Polarization at an Angular Scale of $20'$ ", Astrophys. J. **610**, 625–634, (2004).
7. E. Leitch, J. Kovac, C. Pryke, J. Carlstrom, N. Halverson, W. Holzapfel, M. Dragovan, B. Reddall, E. Sandberg, "Measurement of polarization with the Degree Angular Scale Interferometer", Nature (London) , **420**, 763–771, (2002).
8. S. Masi, P. Cardoni, P. de Bernardis, F. Piacentini, A. Raccanelli, F. Scaramuzzi, "A long duration cryostat suitable for balloon borne photometry", Cryogenics, **39**, 217–224, (1999).
9. November L.J., "Determination of the Jones matrix for the Sacramento Peak Vacuum Tower Telescope", Opt. Eng., **28**, 107–113, (1989).
10. Collett E., *Polarized Light* (M. Dekker Inc., USA, 1993)
11. Max Born and Emil Wolf, *Principles of Optics* (Pergamon Press, 1970)
12. Oscar E. Piro, "Optical properties, reflectance, and transmittance of anisotropic absorbing crystal plates," Phys. Rev. B **36, 6**, 3427 – 3435 (1987).
13. Azzam R.M.A. and Bashara N.M., *Ellipsometry and Polarised Light* (Amsterdam: North-Holland,1977)
14. F. Bréhat, B. Wyncke, "Reflectivity, transmissivity and optical constants of anisotropic absorbing crystals" J. Phys. D: Appl. Phys **24**, 2055 – 2066, (1991).
15. Kraus J.D., *Radio Astronomy* (Cygnus Quasar Books:Powell, OH, 1986)
16. D. Jordan, G. Lewis, E. Jakeman, "Emission polarization of roughned glass and aluminum surfaces," Appl. Opt. **35**, 3583 – 3590 (1996).

17. E. Carretti, R. Tascone, S. Cortiglioni, J. Monari, M. Orsini, "Limits due to instrumental polarisation in CMB experiments at microwave wavelengths", New Ast. **6**, 173–187, (2001).
18. E. Carretti, S. Cortiglioni, C. Sbarra, R. Tascone, "Antenna instrumental polarization and its effects on E- and B-modes for CMBP observations", A&A **420**, 437–445, (2004).
19. C. Bennett, M. Halpern, G. Hinshaw, N. Jarosik, A. Kogut, M. Limon, S. Meyer, L. Page, D. Spergel, G. Tucker, E. Wollack, E. Wright, C. Barnes, M. Greason, R. Hill, E. Komatsu, M. Nolta, N. Odegard, H. Peiris, L. Verde, J. Weiland, "First Year Wilkinson Microwave Anisotropy Probe (WMAP) Observations: Preliminary Maps and Basic Results", Astrophys. J. SS **148**, 1–27, (2003).
20. C. Netterfield, P. Ade, J. Bock, J. Bond, J. Borrill, A. Boscaleri, K. Coble, C. Contaldi, B. Crill, P. de Bernardis, P. Farese, K. Ganga, M. Giacometti, E. Hivon, V. Hristov, A. Iacoangeli, A. Jaffe, W. Jones, A. Lange, L. Martinis, S. Masi, P. Mason, P. Mauskopf, A. Melchiorri, T. Montroy, E. Pascale, F. Piacentini, D. Pogosyan, F. Pongetti, S. Prunet, G. Romeo, J. Ruhl, F. Scaramuzzi, "A Measurement by BOOMERANG of Multiple Peaks in the Angular Power Spectrum of the Cosmic Microwave Background" Astrophys. J. **571**, 604–614, (2002).
21. Afsar M.N., "Precision Dielectric Measurements of Nonpolar Polymers in the Millimeter Wavelength Range" IEEE Trans. Microwave Theory Tech. , MTT-**33, 12**, 1410–1415, (1985).
22. M. Sazhin, G. Sironi, O. Khovanskaya, "Separation of foreground and background signals in single frequency measurements of the CMB polarization" New Ast. **9**, 83–101, (2004).
23. J. Baker-Jarvis, E. Vanzura, W. Kissick, "Improved technique for determining complex permittivity with the transmission/reflection method", IEEE Trans. Microwave Theory Tech. MTT-**38, 8**, 1096–1103, (1990).
24. Jones R.G., "Precise dielectric measurements at 35 GHz using an open microwave resonator", Proc. IEE **123, 4**, 285–290, (1976)
    This proceeding reports the determination of the permittivity and the electric tangent loss of HDPE and Teflon at 35 GHz, by means of a test in which an open microwave resonator is adopted.
25. D. Vaccaneo, R. Tascone, R. Orta, "Adaptive Cavity for Complex Permittivity Measurement of Rock Materials", in *URSI 2004 International Symposium on Electromagnetic Theory*, Proc. of URSI EMTS, 522-524, (2004).
    In this proceeding a new setup based on adaptive cavity for the accurate measurement of the complex permittivity of materials is described.
26. B. Read, J. Duncan, D. Meyer, "Birefringence Techniques for the Assessment of Orientation" Polymer testing, **4**, 143–164, (1984).
27. White J.R., "Origins and Measurement of Internal Stress in Plastics" Polymer testing, **4**, 165–191, (1984).
28. Cortiglioni S., Bernardi G., Carretti E., Casarini L., Cecchini S., Macculi C., Ramponi M., Sbarra C., Monari J., Orfei A., Poloni M., Poppi S., Boella G., Bonometto S., Colombo L., Gervasi M., Sironi G., Zannoni M., Baralis M., Pev-

erini O.A., Tascone R., Virone G., Fabbri R., Natale V., Nicastro L., Ng K-W., Vinyajkin E.N., Razin V.A., Sazhin M.V., Strukov I.A., Negri B., "The Sky Polarization Observatory," New Ast. **9**, 297–327, (2004).

29. Nesti Renzo, "BaR–SPOrt 32 GHz horn design," *CNR–IRA Technical report*, **N. BSPO1.06/03**, 2003.
30. Nesti Renzo, INAF, Largo E. Fermi, 5, 50125 Florence, Italy, (personal communication, 2004).
31. Goldsmith P.F., *Quasioptical System: Gaussian Beam Quasioptical Propagation and Applications*, (Piscataway, N.J.: IEEE Press, 1989)

Table 1. Geometrical sizes of the samples: a is the height, b is the width and l is the length. The dimensions of the WR28 standard rectangular waveguide are: $(a, b) = (3.556, 7.112)$ mm.

	a [mm]	b [mm]	l [mm]
Teflon 1-cut	3.51 ± 0.05	7.10 ± 0.03	59.90 ± 0.07
Teflon 2-cut	3.39 ± 0.09	7.08 ± 0.03	59.85 ± 0.04
HDPE	3.54 ± 0.05	6.93 ± 0.09	60.08 ± 0.10
Polypropylene	3.58 ± 0.03	7.09 ± 0.13	59.98 ± 0.08
Nylon	3.53 ± 0.05	7.11 ± 0.07	60.21 ± 0.13

Table 2. Complex dielectric constant and index of refraction with their maximum errors for: HDPE, Teflon, Polypropylene and Nylon. The values provided are in-band averages (30.4–33.6 GHz).

	$\langle\epsilon_r\rangle_\nu$	$\langle\tan(\delta_e)\rangle_\nu$ $[10^{-4}]$	$\langle n\rangle_\nu$	$\langle\kappa\rangle_\nu$ $[10^{-4}]$
HDPE	2.32 ± 0.03	1.7 ± 0.7	1.523 ± 0.010	1.30 ± 0.54
Teflon	2.04 ± 0.02	1.6 ± 0.4	1.428 ± 0.007	1.14 ± 0.29
Polypropylene	2.24 ± 0.03	4.6 ± 1.8	1.497 ± 0.010	3.44 ± 1.37
Nylon	3.00 ± 0.02	111.0 ± 1.7	1.732 ± 0.006	96.13 ± 1.79

Table 3. In band (30.4–33.6 GHz) variation, with respect to their average value, of ϵ_r and $\tan(\delta_e)$ for HDPE, Teflon, Polypropylene and Nylon.

	η_{ϵ_r}	$\eta_{\tan(\delta_e)}$
HDPE	0.2 %	30 %
Teflon	0.1 %	25 %
Polypropylene	0.1 %	10 %
Nylon	0.2 %	2 %

Table 4. Bibliographic data of complex dielectric constants for HDPE, Teflon and Polypropylene. The last column refers to bibliography. No datum is available for Nylon.

	ν [GHz]	ϵ_r	$\tan(\delta_e)$	Reference
HDPE	35.26	2.359	0.00017	[24]
Teflon	34.54	1.95	0.00005	[24]
Polypropylene	35	2.254	0.00015	[21]

Table 5. In-band average (30.4–33.6 GHz) with their maximum errors of the complex dielectric constant and index of refraction for both 1-cut and 2-cut Teflon. The parameters $\langle \tan(\delta_e) \rangle_\nu$ and $\langle \kappa \rangle_\nu$ are in $[10^{-4}]$ units. Last two columns report the in band variation of $\epsilon_{\mathbf{r}}$.

	$\langle \epsilon_r \rangle_\nu$	$\langle \tan(\delta_e) \rangle_\nu$	$\langle n \rangle_\nu$	$\langle \kappa \rangle_\nu$	η_{ϵ_r}	$\eta_{\tan(\delta_e)}$
1-cut	2.04 ± 0.02	1.6 ± 0.4	1.428 ± 0.007	1.14 ± 0.29	± 0.1 %	± 25 %
2-cut	2.01 ± 0.02	2.2 ± 0.7	1.418 ± 0.007	1.56 ± 0.50	± 0.1 %	± 10 %

Table 6. Conservative estimates of the noise temperature introduced by the flat dielectric slab evaluated at $\mathrm{T}_{\mathrm{ph}}^{\mathrm{MAX}} = 300$ K. The thickness d_0 is 0.33 cm for Teflon, 0.31 cm for HDPE and Polypropylene.

	$\langle \varepsilon(d,\nu,\theta) \rangle_\nu \vert_{\mathrm{MAX}(\theta)}$	$\mathrm{T}_A^\varepsilon(d)/\mathrm{T}_{\mathrm{ph}}^{\mathrm{MAX}}$	$\mathrm{T}_{\mathrm{noise}}$ [mK]
Teflon	6.1×10^{-4}	5.4×10^{-4}	162
HDPE	6.6×10^{-4}	5.9×10^{-4}	177
Polypropylene	17.0×10^{-4}	15.4×10^{-4}	462

Table 7. Upper limits of the spurious polarization as from Eq. (51) introduced by HDPE, Teflon and Polypropylene isotropic slab. The thickness adopted is d_0. $\Delta T_b^{MAX} = 100\mu K$ and $\Delta T_{ph}^{MAX} = 1$ K. (The same for U).

	$SP^T_{\rm MAX}$	$Q^T_{SP}\|_{\rm MAX}$	$SP^\varepsilon_{\rm MAX}$	$Q^\varepsilon_{SP}\|_{\rm MAX}$	$Q_{SP}\|_{\rm MAX}$
HDPE	0.240	24 μK	0.00015	0.15 mK	0.174 mK
Teflon	0.215	$\sim$ 22 μK	0.00012	0.12 mK	0.142 mK
Polypropylene	0.235	$\sim$ 24 μK	0.00038	0.38 mK	0.404 mK

Table 8. Upper limits of the spurious polarization, as from Eq. (53)-(54), introduced by HDPE, Teflon and Polypropylene isotropic slab by taking into account the BaR-SPOrt feed. The thickness adopted is d_0. $\Delta T_b^{MAX} = 100\mu K$ and $\Delta T_{ph}^{MAX} = 1$ K. (The same for U).

	$\|Q^T_{SP}\|/\Delta T_b^{MAX}$	$Q^T_{SP}\|_{\rm MAX}$	$\|Q^\varepsilon_{SP}\|/\Delta T_{ph}^{MAX}$	$Q^\varepsilon_{SP}\|_{\rm MAX}$	$Q_{SP}\|_{\rm MAX}$
HDPE	3.1×10^{-5}	0.0031 μK	8.8×10^{-7}	0.88 μK	$\sim$ 0.9 μK
Teflon	2.6×10^{-5}	0.0026 μK	6.0×10^{-7}	0.60 μK	$\sim$ 0.6 μK
Polypropylene	3.7×10^{-5}	0.0037 μK	18.8×10^{-7}	1.88 μK	$\sim$ 1.9 μK

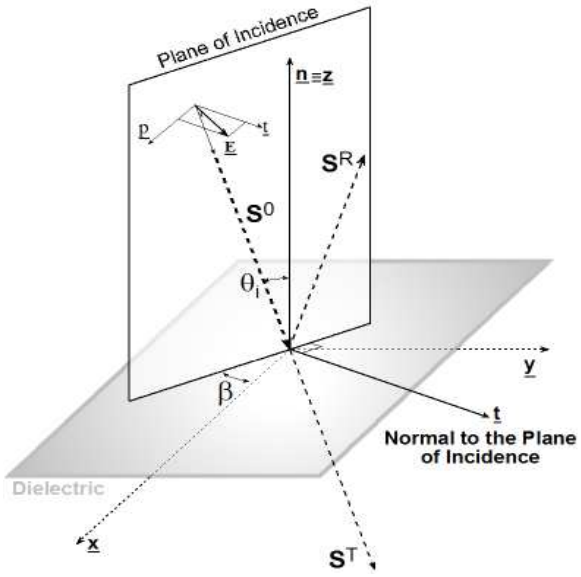

Fig. 1. Reference frame: $\underline{\mathbf{x}}$, $\underline{\mathbf{y}}$ and $\underline{\mathbf{z}}$ define the laboratory or feed-horn reference frame. β is the angle between the plane of incidence and the $\underline{\mathbf{x}}$ axis.

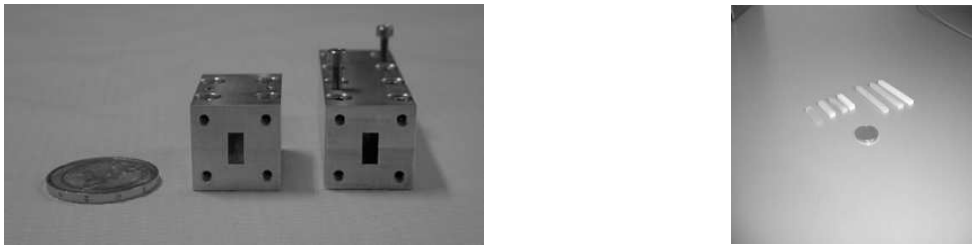

Fig. 2. Waveguides and dielectric samples.

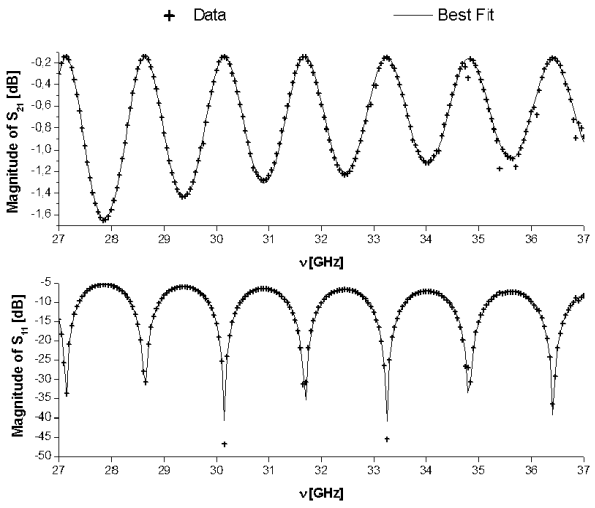

Fig. 3. Measurements (+) and best fit (—) of scattering parameters of the Teflon 1-cut loaded waveguide.

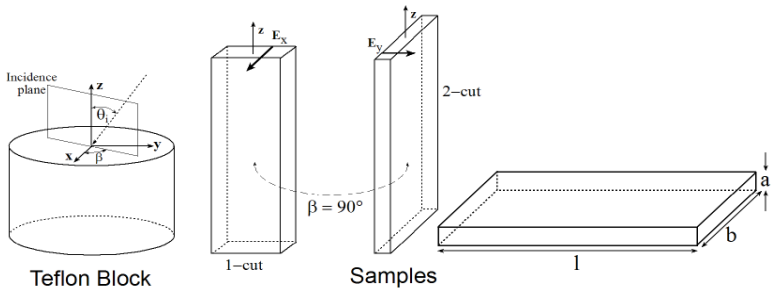

Fig. 4. Dielectric cuts. $\mathbf{E}_x$ and $\mathbf{E}_y$ are the electric field components vibrating along the **x** and **y** directions in the Antenna Reference Frame. a, b and l denote the sample sizes. 1–cut and 2–cut refers only to Teflon. See text for details.

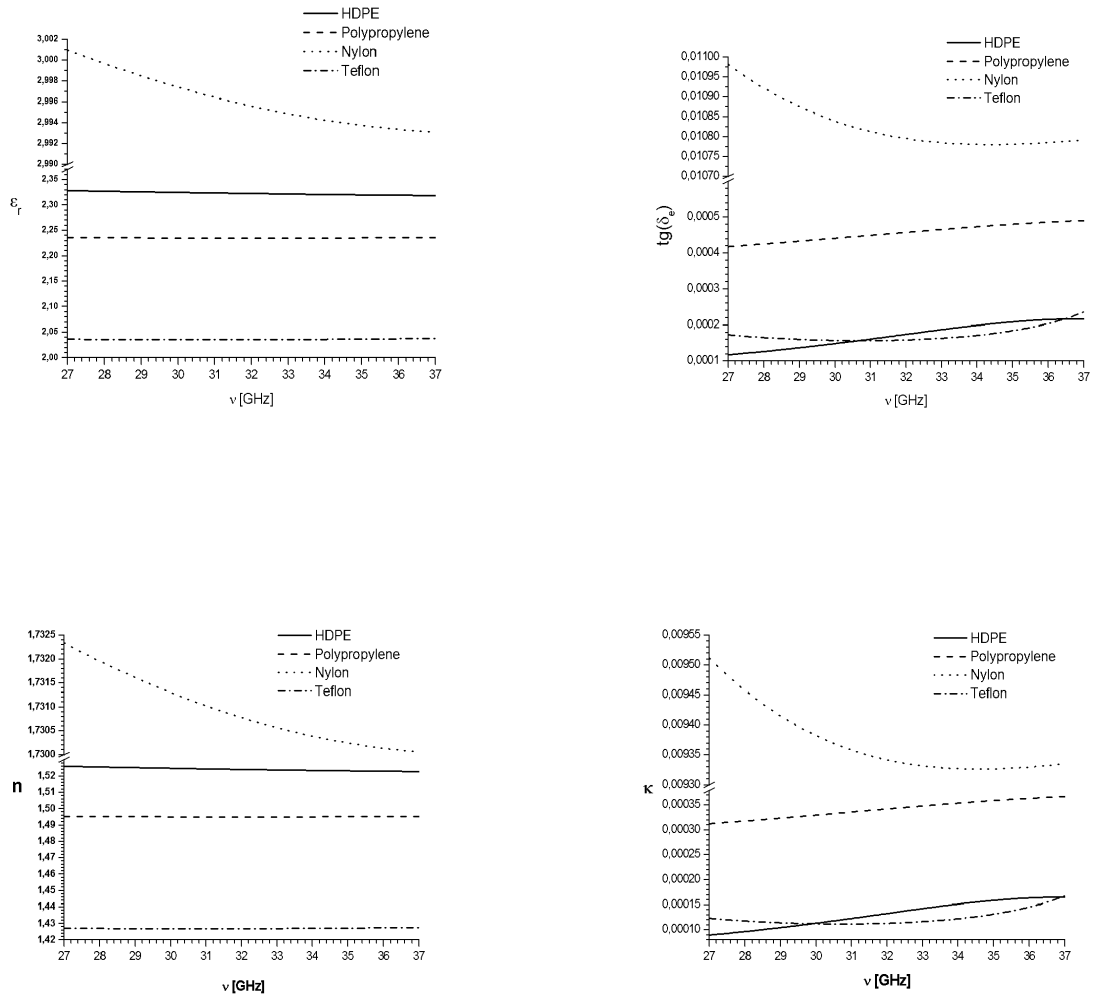

Fig. 5. Complex dielectric constant and index of refraction of: HDPE, Polypropylene, Nylon and 1–cut Teflon. The measurements have been performed at $T_{ph} = 300$ K with $\sim 1\%$ of precision for ϵ_r and n, and $\sim 30\%$ for $\tan(\delta_e)$ and κ (only for Nylon is 1%).

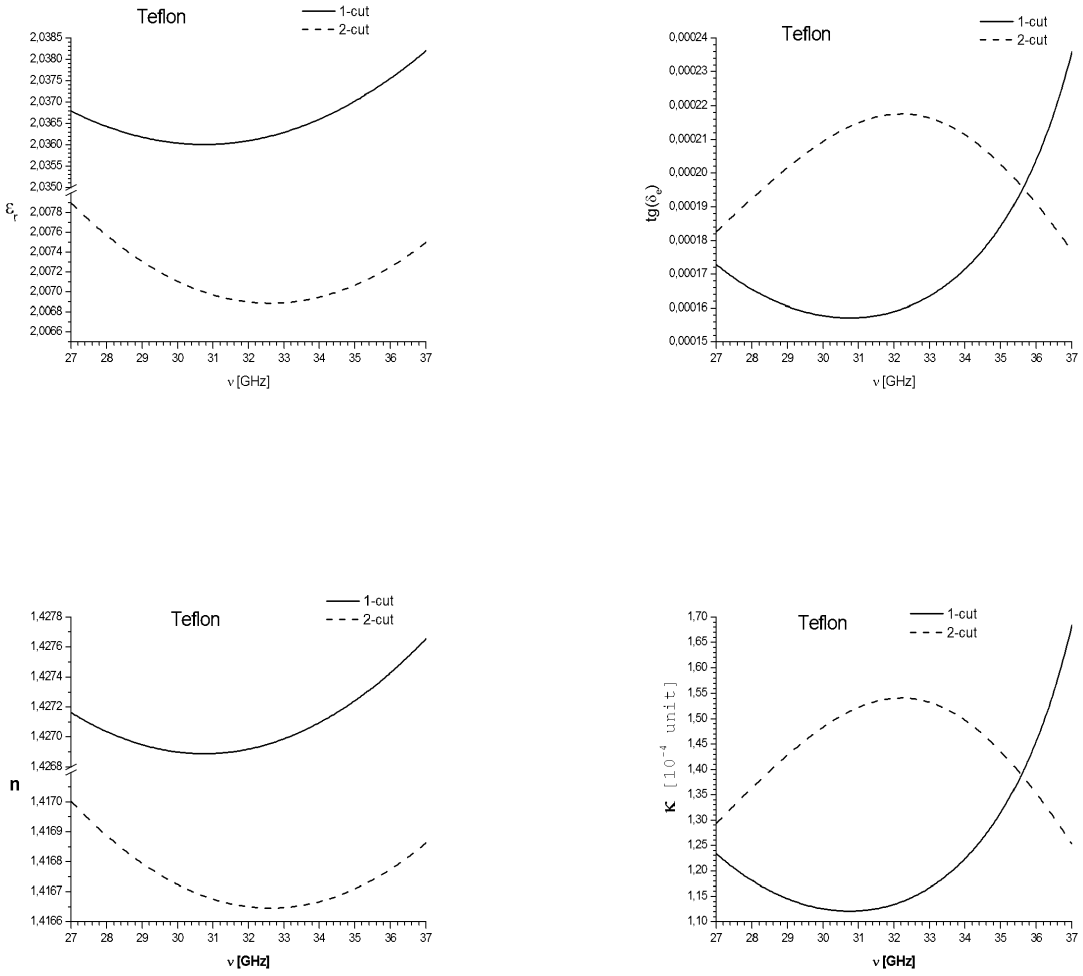

Fig. 6. Complex dielectric constant and index of refraction of 1–cut and 2–cut Teflon. The measurements have been performed at $T_{ph} = 300$ K. The precision for ϵ_r and n is $\sim 1\%$, and for $\tan(\delta_e)$ and κ is $\sim 30\%$.

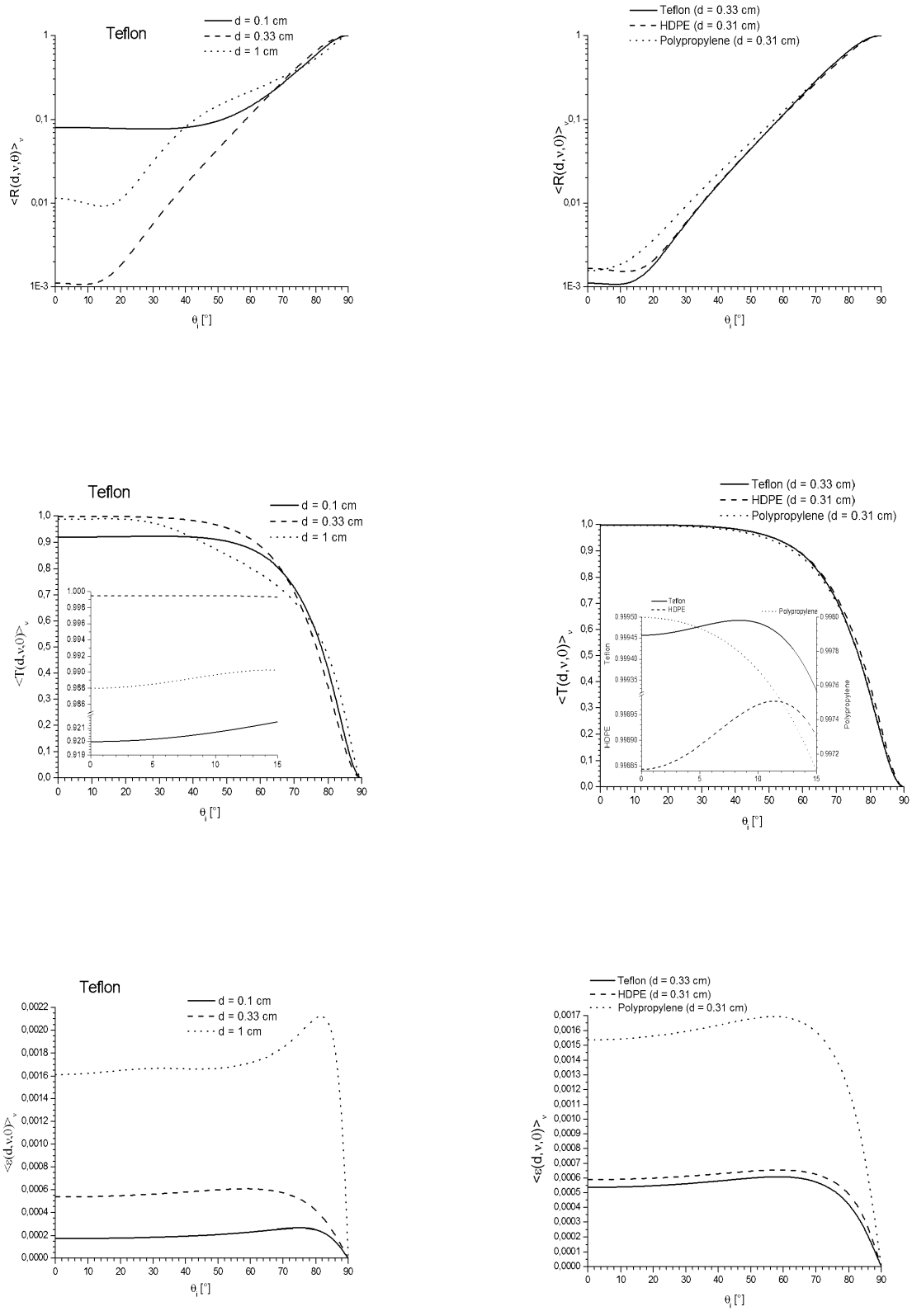

Fig. 7. In band average reflectance, transmittance and emittance. Left: Teflon. Right: comparison among dielectrics. d is the slab thickness.

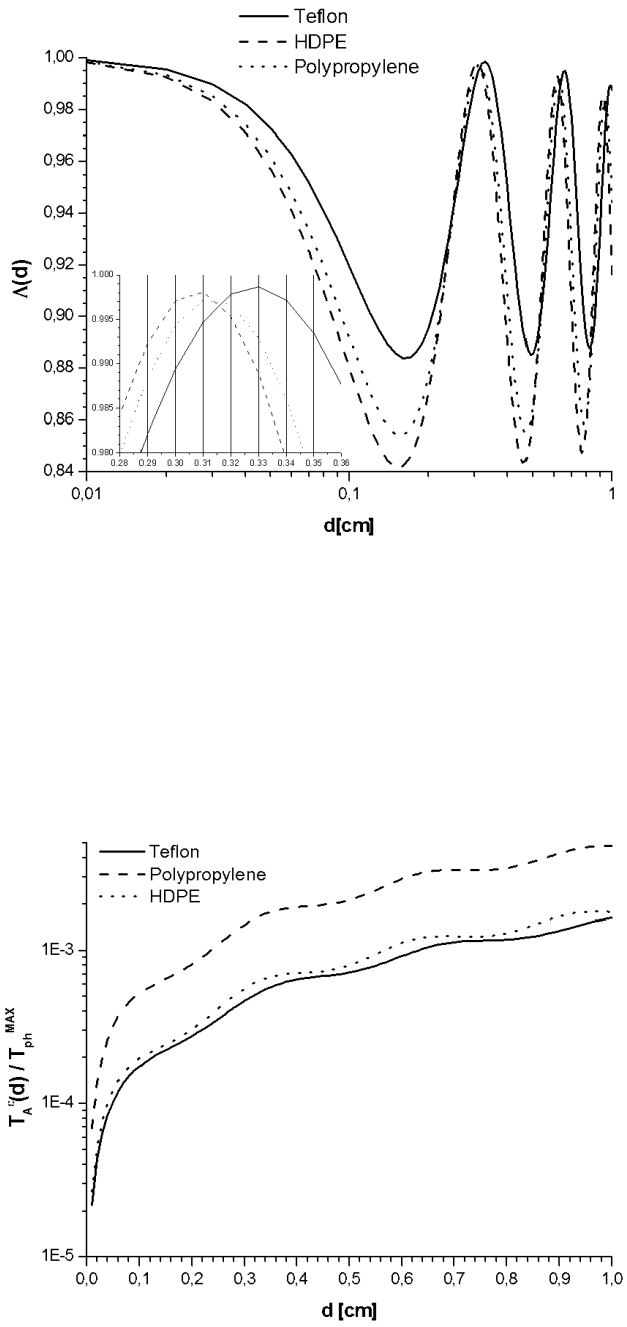

Fig. 8. BaR-SPOrt case. Top: the relative transmitted signal Λ. Bottom: upper limit of the relative emitted signal. d is the slab thickness.

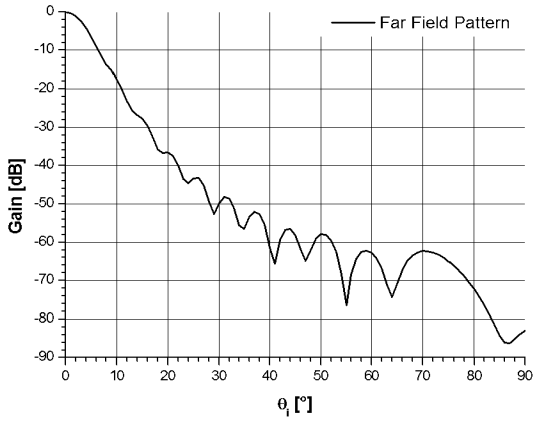

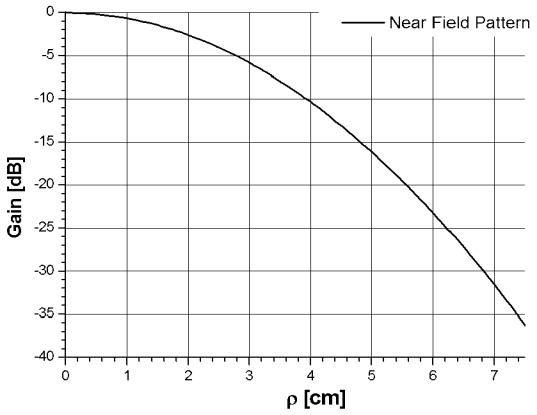

Fig. 9. Left: BaR-SPOrt far field patterns. Right: the near field versus the radial coordinate from the circular flat slab center ($\rho \leq$ R = 7.5 cm, where R is the radius), by assuming a Gaussian beam approximation and using the following system parameters: distance between the feed aperture and the slab (δ = 6.5 mm); confocal distance (z_c = 204.56 mm); waist (w_0 = 24.707 mm) and the distance between the waist and the slab (z = 224.716 mm) (see Ref. 29, 30).

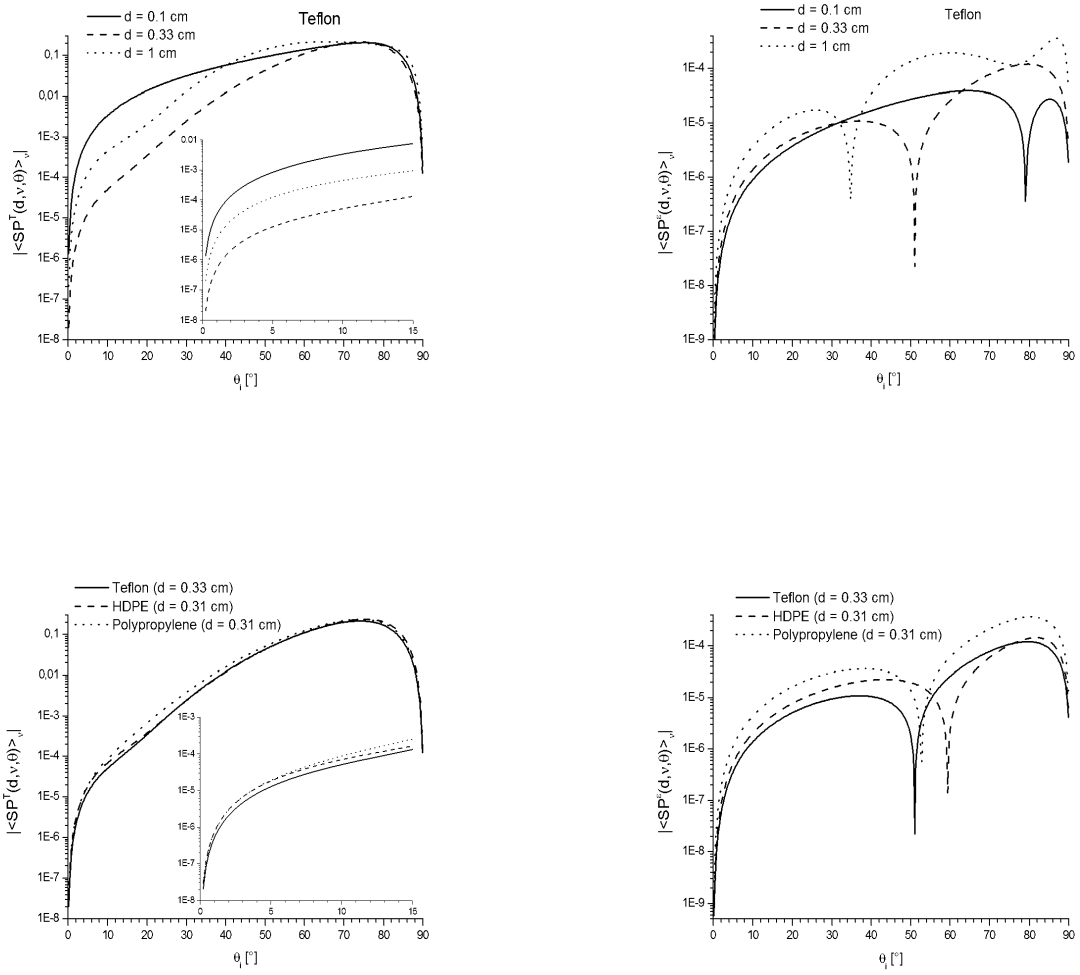

Fig. 10. Absolute value of the spurious polarization coefficients related to Teflon, HDPE and Polypropylene in the 30.4–33.6 GHz band. Left: transmission regime. Right: emission regime. d is the slab thickness.

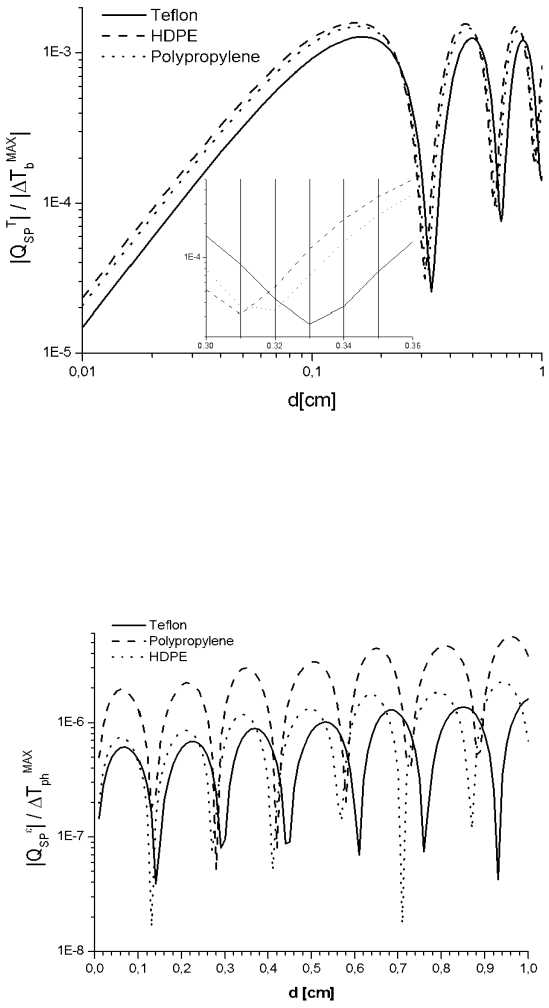

Fig. 11. BaR-SPOrt case. Top: upper limit of the spurious polarized transmission. Bottom: upper limit of the spurious polarized emission. (Similarly for U). d is the slab thickness.

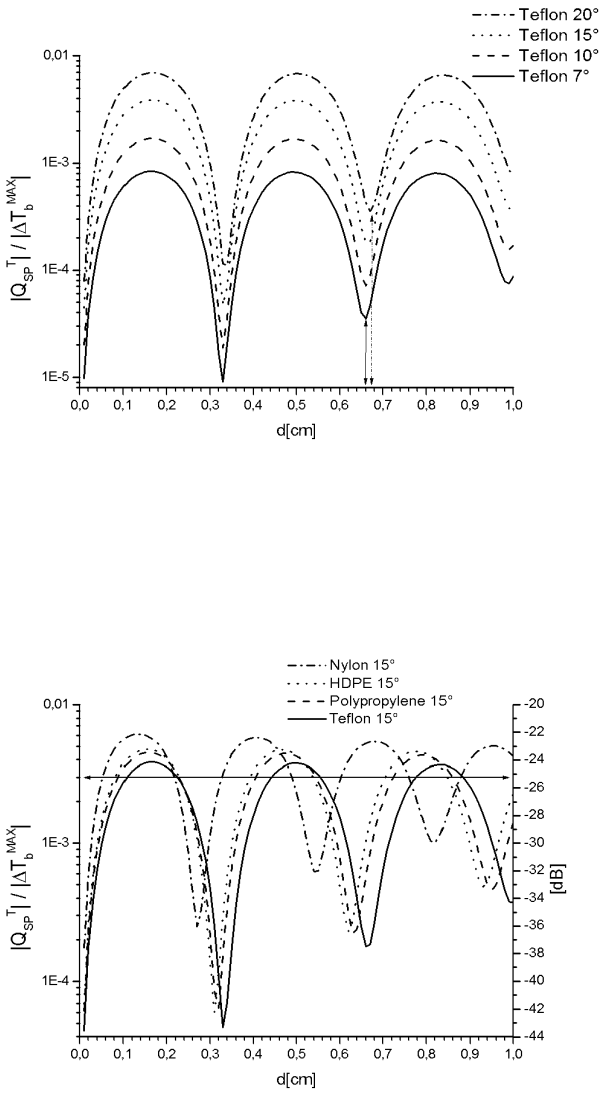

Fig. 12. Plots of the spurious polarization transmitted by flat dielectrics in far field regime, in the 30.4–33.6 GHz band, by increasing the beam pattern. Nylon is shown only for comparison. d is the slab thickness. See text for details.

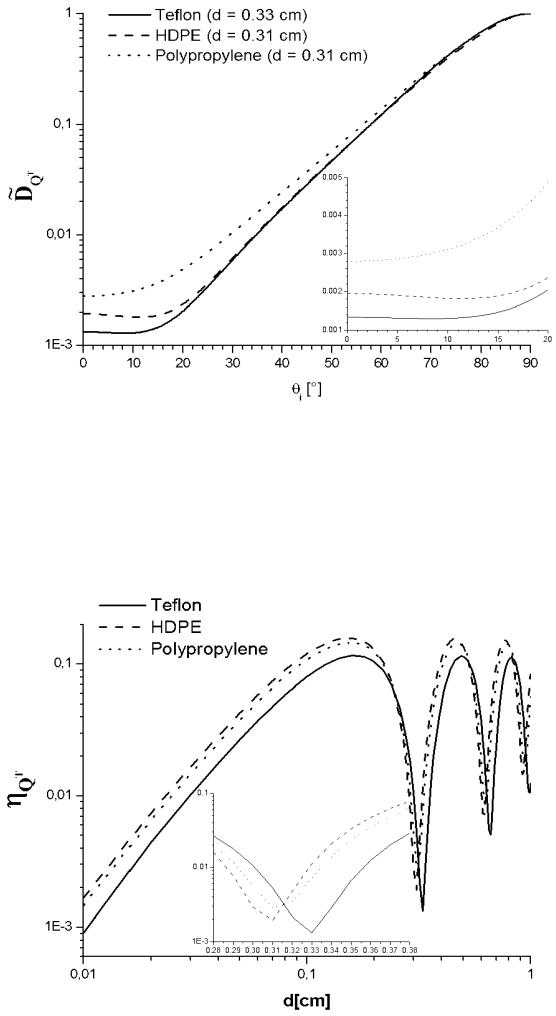

Fig. 13. Plots of the $\tilde{D}_Q^T$ term (top) and of the depolarization in transmission regime (bottom) introduced by Teflon, HDPE and Polypropylene in the 30.4–33.6 GHz band. d is the slab thickness.

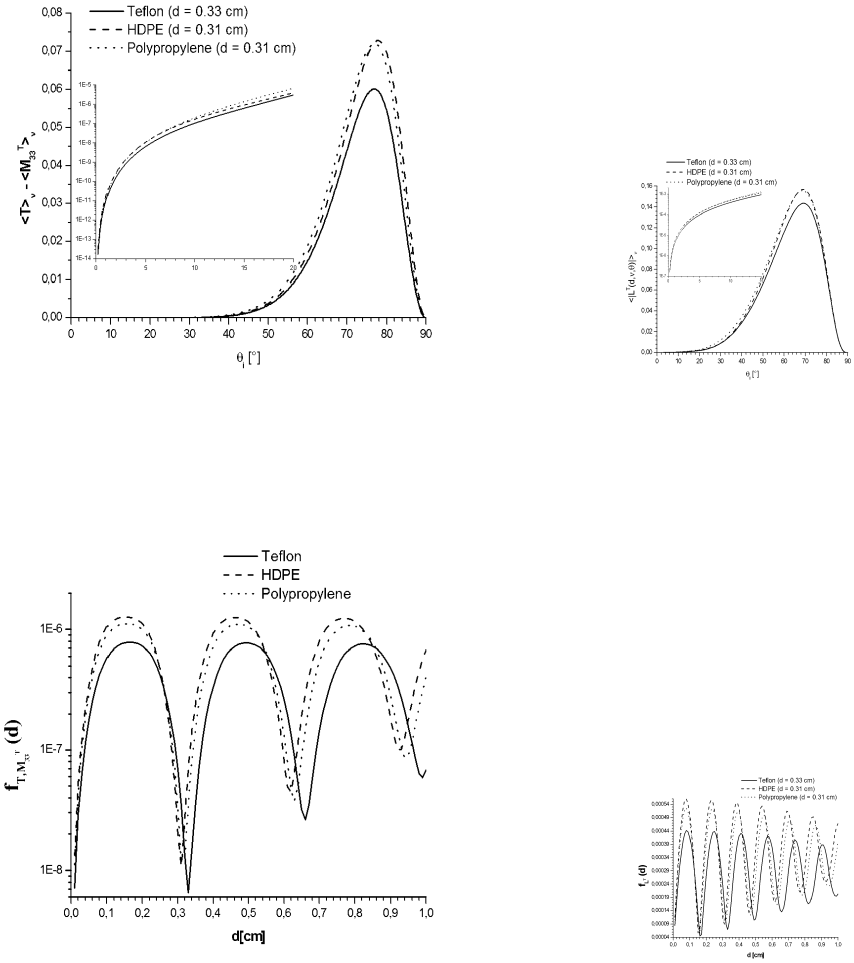

Fig. 14. Plots of the leakage effects for Teflon, HDPE and Polypropylene in the 30.4–33.6 GHz band. Bottom plots are for the BaR–SPOrt case. d is the slab thickness.